Passive Systems Theory with Narrow-Band and Linear Constraints: Part I–Spatial Diversity

JOSÉ M. F. MOURA AND ARTHUR B. BAGGEROER, MEMBER, IEEE

Abstract–This paper studies passive problems where the receiver extracts from the source radiated signature information concerning the parameters defining the relative source/receiver geometry.

A model encompassing the fundamental global and local characteristics for passive positioning and navigation is presented. It considers narrow-band signals, imposes linear constraints on the geometry, and exhibits explicitly the symmetry between the space and time aspects. The analysis concentrates on questions of global geometry identifiability, emphasizing the passive global range acquisition.

The maximum-likelihood processor is analyzed by studying the ambiguity structure associated with inhomogeneous passive narrow-band tracking. Bounds on the global and local mean-square error performance are studied and tested via Monte Carlo simulations. By considering two limiting geometries, a distant and a close observer, simple approximate expressions for the mean-square errors are presented and compared to the exact bounds.

Herein the study is restricted to stationary geometries where the source is located by an extended array (spatial diversity). Subsequent papers generalize the study to moving sources (temporal diversity) and to coupled geometries.

I. INTRODUCTION

IN MANY tracking problems the observers are of the passive type, capable only of receiving waves without control over them. These passive systems are relevant in a variety of fields: oceanography (locating drifting buoys) [18], [21], meteorology (tracking radiosondes or balloon-borne devices) [9], passive sonar (positioning submersibles, commercial fish finders) [1], nagivation (obtaining position fixes, collision avoidance systems) [10], and so forth.

Fig. 1 shows typical navigational configurations. In Fig. 1 (a) and (c) an omnidirectional receiver R determines its position relative to an ensemble of beacons $B_1, \cdots, B_N$, or relative to a moving satellite. In Fig. 1(b) and (d) a fixed extended platform R_1 to R_N or a moving omnidirectional receiver uses a single beacon as positional reference. Geometries (a) and (b) are stationary; the basic characteristic is the spatial separation exhibited by the source or the receiver. Configurations (c) and (d) are not fixed; the spatial separation observed is synthetically generated by the relative motions. Generally the navigational problem is complex, inducing on the signal a space/time coupled diversity structure.

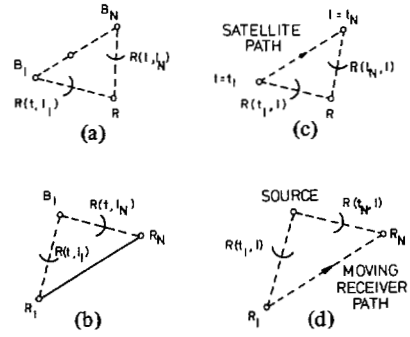

Fig. 1. Typical navigational configurations: (a) Extended source (beacons B_1 to B_N). (b) Extended receiver. (c) Moving source. (d) Moving receiver.

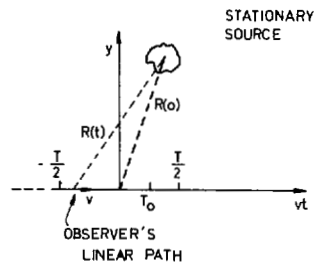

Fig. 2. Passive tracking global geometry.

Reversing the roles in the preceding navigation examples, a positioning application is obtained. In the latter it is the stationary or moving receiver, of known position and dynamics, that tracks a stationary or moving source. Given the dualism, the discussion is restricted to positioning problems.

In Fig. 2, the distance between the source and the linear array's geometric center has the parabolic form of Fig. 3(a), thereby inducing the time variant Doppler modulation indicated in Fig. 3(b). Observation of the change in frequency of the wave emitted by the moving source enables measurement of its speed (Doppler phenomenon). But, at point T_0 of the stationary Doppler modulation (closest point of approach), the line defined by the array's geometric center and the source is normal to the path. Many practical positioning and navigational techniques use this elementary observation.

This paper, and the accompanying Parts II [14] and III [15], are concerned with performance analysis and design of

Manuscript received March 16, 1977; revised June 15, 1977. This work was supported by the J.S.E.P., under Contract DAAB07-71-C-0300.

J. M. F. Moura is with Centro De Análise e Processamento de Sinais, Complexo Interdisciplinar and the Department of Electrical Engineering, Instituto Superior Técnico, Lisboa-1, Portugal.

A. B. Baggeroer is with Research Laboratory of Electronics and the Department of Electrical Engineering and Computer Science at M.I.T., Cambridge, MA 02139.

0364-9059/78/0100-0005$00.75 © 1978 IEEE

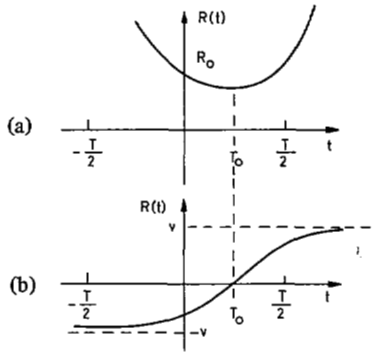

Fig. 3. Doppler modulation induced on the temporal signal structure. (a) Range history. (b) Doppler modulation.

receivers extracting from the signal's structure all available information concerning the source position and dynamics. The study concentrates on the global identifiability of the parameters, with emphasis on the range acquisition. Part I analyzes problems where the geometry is stationary (no relative dynamics), e.g., as in triangulation with an extended source (navigation) or an extended array (positioning). Part II [14] considers those applications where both the source and the observer are pointwise, as, for example, in Doppler location with a single beacon (navigation) or with an omnidirectional array (positioning). Finally, Part III [15] studies the situations where the signal has a spatial and a temporal structure, concentrating on the resulting coupling issues. In [12] this theory is applied to the design of algorithms achieving global acquisition and tracking for passive positioning and navigation problems of practical significance.

II. PRELIMINARY CONSIDERATIONS ON PASSIVE TRACKING

There are two modeling issues. The first involves the signal structure; the second concerns the global geometry and the relative dynamics.

The study is here restricted to the following.

1) A class of random wave forms, in which narrow-band signals multiplied by a Rayleigh-Gaussian random parameter are observed, imbedded in an additive, spatially homogeneous, temporally white Gaussian noise process.

2) A planar geometry with linear constraints. The receiving antenna is either omnidirectional or linear and the source/receiver dynamics are either stationary (with no relative motions) or linear (e.g., source following a deterministic constant-speed linear path). In [12] a more realistic model is discussed where the linear path is disturbed by random accelerations.

Under the preceding assumptions the resulting wave form distribution exhibits in time and space a "narrow-band" modulated structure, and thus is temporally nonstationary and spatially inhomogeneous.

Although the ideal tracking system would use all available information conveyed by the received wave forms the analysis is concentrated on the phase modulations of the narrow-band signals. In particular, the observed changes in the signal strength occurring either across the extended receiving antenna or during the finite time observation interval are ignored. These are of practical significance only, for example, when the total array dimensions are much larger than the source/receiver separation and hence represent higher order corrections that will not be pursued. However the model does take into account transmission losses due to fading, internal wave phenomenon, and medium inhomogeneities, by considering, besides an additive measurement noise, a multiplicative random-type disturbance (Rayleigh channel).

Narrow-band passive tracking has received considerable attention [7], [11], [17]. In most of the studies the following three assumptions are made.

S1. Far-field geometry: The wavefronts are assumed planar; the global and/or local wavefront curvature is neglected.

S2. Decoupling: The spatial and temporal processing aspects are decoupled.

S3. Finite parameter context: The relative source/receiver dynamics are stationary or deterministic. Passive tracking is reduced to a finite parameter estimation problem.

Under S1-S3 the problem simplifies to a "bearings only" situation, wherein the observable source/receiver parameter is the bearing angle and/or the source (radial) velocity. Ranging is accomplished either by an auxiliary active system or by *ad hoc* procedures such as simple triangulation or Doppler counting.

As far as we know, some preliminary analytical work taking into account the (spatial) curvature of the waveforms has only recently been reported [4], [5]; moreover, inhomogeneous waveforms have received scant attention in other applied areas. An exception is in optics [8] where quadratic approximations to the waveform curvature are usual in Fresnel diffraction studies. Also in seismic profiling, new techniques [3], [19] explore the signal's nonlinear spatial structure. Wave theory is still another area which considers a mixture of plane and inhomogeneous waves when finding the distribution of a field scattered by a rough surface [2].

Passive narrow-band tracking when only S1 is assumed has previously been studied [13]. The motions were modeled by a stochastic finite-dimensional dynamic system. A spatial/time integrated approach, with planar wavefront structure, was developed based on first-order approximations to the infinite-dimensional filter. Analysis substantiated by Monte Carlo simulations showed that the filter tracked only the local dynamics and lacked global range observability. This set of papers explores the spatially inhomogeneous and/or the temporally nonstationary character of the waveforms (spatial and temporal curvature). The absence of the hypothesis S1 is an underlying characteristic of the study.

With the point source emitting $S(t)$, the signal at a sensor with spatial coordinate l, and at time t is

$$s(t, l) = S(t - \tau(t, l)) \tag{1}$$

where $\tau(t, l)$ is the travel time delay. For a homogeneous medium

$$\tau(t, l) = \frac{R(t - \tau(t, l))}{c} \cong \frac{R(t, l)}{c} \tag{2}$$

where $R(t, l)$ is the source/sensor separation and c the medium propagation velocity.

In the present paper the geometry is stationary. The signal exhibits a spatial diversity structure

$$\tau(t, l) = \tau(l) \tag{3}$$

i.e., the delay is independent of the time variable. In Part II [14] the signal for processing presents a temporal diversity structure, i.e.,

$$\tau(t, l) = \tau(t). \tag{4}$$

Finally, Part III [15] considers more general geometries, where space and time coupling arise.

III. STATIONARY SOURCE MODEL

Fig. 4(a) illustrates the parametrization for a planar geometry where a stationary point source is being tracked by a linear array oriented along the l axis. Fig. 4(b) shows the problem where a moving omnidirectional sensor (e.g., a short or nonlinear array) with known speed v locates a stationary source. These passive tracking geometries, being space and time dual versions of the same problem, are discussed in the context of the first one. In the sequel they are simply referred to as synthetic observer/stationary source (SOSS) problems.

The distance from the source to the array element at location l is given by the range function

$$R(t, l, A) = \{R_0^2 + l^2 - 2lR_0 \sin\theta\}^{1/2},$$

$$l \in \left[-\frac{L}{2}, \frac{L}{2}\right], \qquad t \in \left[-\frac{T}{2}, \frac{T}{2}\right]. \tag{5}$$

In (5)

$$A = [R_0 \sin\theta]^T \tag{6}$$

is the parameter vector defining the relative geometry; it is modeled as unknown and nonrandom. In (6) T denotes matrix transposition.

The source radiates narrow-band signals, which are received across the observing antenna as

$$r(t, l) = \sqrt{2}\, Re\{\tilde{r}(t, l) \exp j\omega_c t\} \tag{7}$$

where

$$\tilde{r}(t, l) = \tilde{s}(t, l, A) + \tilde{w}(t, l) \tag{8}$$

$\tilde{w}(t, l)$ is a zero mean, spatially and temporally "white," Gaussian noise with double spectral height of N_0. The signal complex envelope is

$$\tilde{s}(t, l, A) = \sqrt{E_r}\tilde{b}\tilde{s}_n(t, l, A) \tag{9}$$

with $\tilde{s}_n(t, l, A)$ being a normalized signal

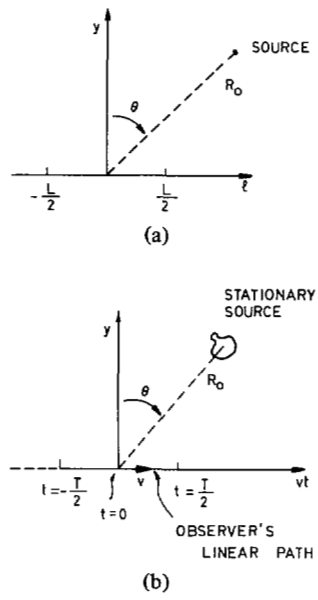

Fig. 4. Planar geometry for a stationary source: (a) Stationary array. (b) Moving omnidirectional array.

$$\tilde{s}_n(t, l, A) = \frac{1}{\sqrt{LT}} \exp\left[-j\frac{2\pi}{\lambda}R(t, l, A)\right],$$

$$t \in \left[-\frac{T}{2}, \frac{T}{2}\right], \qquad l \in \left[-\frac{L}{2}, \frac{L}{2}\right]. \tag{10}$$

$E_r = PLT$ = total energy received during the observation interval $[-T/2, T/2]$, by an array of geometric dimension L; P = signal power; $\lambda = c/f = 2\pi c/\omega_c$ = wavelength; f = carrier frequency; c = medium waveform speed propagation. $\tilde{b} = b \exp j\psi$, with b Rayleigh and ψ uniformly distributed random variables.

The zero mean Gaussian random variable $\tilde{b}$, with variance $E|\tilde{b}|^2 = 2\sigma_b^2$ independent of the measurement noise $\tilde{w}(t, l)$, accounts for model inaccuracies, e.g., radiated signal power variations about some nominal value, fading in the transmission medium, etc. More importantly, the presence of $\tilde{b}$ in (9) represents a structural model constraint: the lack of knowledge of the signal absolute phase (incoherent receiver). It precludes the estimation of the travel time delay, which measures the range in synchronized systems [6]. The paper studies then alternative procedures for range acquisition exploring the signal nonlinear phase structure.

IV. AMBIGUITY STRUCTURE

Under the model assumptions of Section III, the optimum receiver is a maximum-likelihood (ML) processor, e.g. [20], chapter X; it maximizes a monotonic function of the ML function on the parameter space Ω

$$\ln \Lambda_1(\bar{A}) = \frac{1}{N_0}\frac{\bar{E}_r/N_0}{1 + \bar{E}_r/N_0}|\tilde{L}(\bar{A})|^2 \tag{11}$$

where

$$\bar{E}_r = \text{average received energy} = (2\sigma_b{}^2)E_r \tag{12}$$

and

$$\tilde{L}(\bar{A}) = \int_{-T/2}^{T/2} dt \int_{-L/2}^{L/2} dl\, \tilde{r}(t, l)\bar{s}^*(t, l, A). \tag{13}$$

With an inner product notation

$$\tilde{L}(\bar{A}) = \langle \tilde{r}, \bar{s}(\bar{A}) \rangle. \tag{14}$$

$L(\bar{A})$ is a Gaussian random variable, with statistics

$$E\tilde{L}(\bar{A}) = \langle \bar{s}(A), \bar{s}(\bar{A}) \rangle \tag{15}$$

$$E\{ [\tilde{L}(A_1) - E\tilde{L}(A_1)] [\tilde{L}(A_2) - E\tilde{L}(A_2)]^* \}$$
$$= \langle \bar{s}(A_1), \bar{s}(A_2) \rangle \tag{16}$$

where A is the actual source vector, and A_1, A_2 are scanning parameter values.

A practical procedure in two steps maximizes (11) over the continuous parameter space Ω. In the first stage Ω is made discrete by a grid; the vertex at which the ML function is maximum is chosen as a coarse estimate. In the second stage a finer search about the previous value returns the approximate ML estimate A_{ml}.

Like in active radar, the structure of the signal autocorrelation

$$\Psi(A, \bar{A}) \triangleq \langle \bar{s}_n(A), \bar{s}_n(\bar{A}) \rangle \tag{17}$$

and its squared modulus, the generalized ambiguity function (GAF)

$$\Phi(A, \bar{A}) = |\Psi(A, \bar{A})|^2 \tag{18}$$

play an important role in dimensioning the grid and evaluating the algorithm's mean square performance (see (15) and (16)). In (17) the index n indicates that the signal normalized version (10) is used.

In (11)-(18) the statistical assumptions are reflected in the multiplying gain, while the geometry affects the GAF structure. This factoring is a result of the signal and noise model assumed.

Basically the following two issues have to be pursued.

1) The GAF's main lobe structure, i.e., its local description on Ω about the source location.

2) The GAF's secondary structure, i.e., its relative maxima global distribution, size and rate of falloff. These points are studied next, using first an approximation to GAF and then the general expression (18).

A. Approximate Analysis

The analysis of the GAF is carried out by assuming a polynomial approximation to the phase range difference defined in (19). For a source in the so-called Fresnel zone, a second-order expansion is appropriate leading to

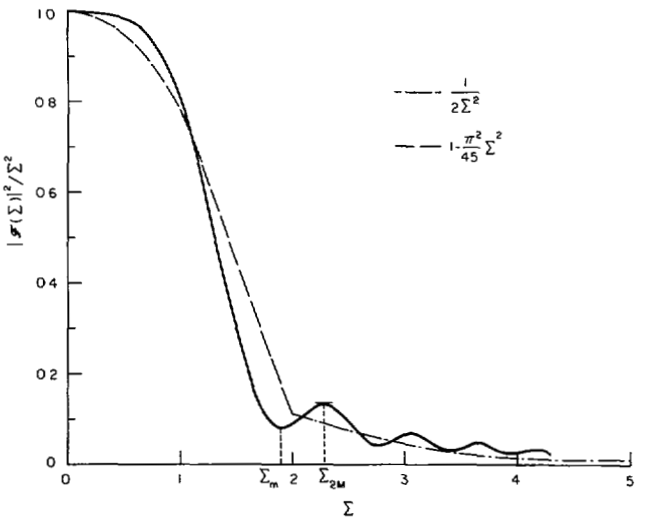

Fig. 5. Ambiguity Fresnel structure.

$$\Delta R(l, A, \bar{A}) \triangleq R(l, A) - R(l, \bar{A}) = \sum_{i=0}^{n} \Delta_i l^i \tag{19}$$

$$= \Delta R_0 - \Delta \sin\theta\, l + \Delta\left(\frac{\cos^2\theta}{R_0}\right)\frac{l^2}{2} \tag{20}$$

where $\Delta_0 = \Delta R_0 = R_0 - \bar{R}_0$ and likewise for the remaining quantities in (19) and (20). For the quadratic phase (20), the GAF is

$$\Phi(A, \bar{A}) \cong \frac{1}{\Delta\Sigma}[F(\Sigma_+) - F(\Sigma_-)]^2 \tag{21}$$

where

$$\Delta\Sigma = \Sigma_+ - \Sigma_-, \Sigma_\pm = \left(\pm\frac{L}{2} + \frac{\Delta_1}{2\Delta_2}\right)$$

$$F(\Sigma) = \int_0^\Sigma \exp jt^2\, dt = \text{Fresnel exponential integral.}$$

Along the $\Delta_1 = \Delta \sin\theta$ axis the GAF has the sinc-squared structure[1]

$$\Phi(A, \bar{A}) = \text{sinc}^2\left[\frac{2\pi}{\lambda}\Delta \sin\theta\, \frac{L}{2}\right] \tag{22}$$

whose second largest global maximum is reduced to about 4.5 percent of the value at the origin.

Along the radial $\Delta(\cos^2\theta/R_0)$ axis it has the Fresnel structure

$$\Phi(A, \bar{A}) = |F(\Sigma)/\Sigma|^2 \tag{23}$$

[1] $\text{sinc}\, X = \sin X/X$.

illustrated in Fig. 5, with second maximum equal to 0.132 and where $\Sigma = [(\pi/\lambda)\Delta(\cos^2\theta/R_0)]^{1/2}L/2$. Fig. 5 presents also local (about $\Sigma = 0$) and asymptotic (large Σ) quadratic expansions approximating the Fresnel ambiguity structure (23). Equivalent graphical displays may be obtained for (21). However the two-dimensional studies are carried out with the exact expression for the GAF.

B. Graphical Analysis

Fig. 6 presents a three-dimensional and a contour plot of the GAF for the actual source values $A_a = [0.6 \times 10^5 \text{ ft} \quad \sin 15^\circ]^T$, and an array $L = R_0/2$. Equivalent diagrams for distant (small array) and close (large array) observers are in [12]. These figures display elliptical patterns for the main-lobe equal-height contours and negligible secondary peaks (less than 20 percent of the GAF's maximum value). An asymptotic analysis, based on the method of stationary phase, e.g. [16], is pursued in [12] leading to bounds on the GAF's rate of falloff similar to the one shown in Fig. 5.

V. MAIN-LOBE QUADRATIC DESCRIPTION

The elliptical patterns of Fig. 6(b) legitimize a quadratic analysis of the GAF's main lobe. Retaining terms up to the second order in the Taylor's series expansion

$$\Phi(A, A_a) \cong 1 - \Delta A^T M \Delta A \tag{24}$$

where $\Delta A = A - A_a$, and

$$M = [M_{ij}] = -\frac{1}{2}\left[\frac{\partial^2 \Phi(A, A_a)}{\partial A_i \partial A_j}\bigg|_{A=A_a}\right] \tag{25}$$

is defined as the mean-square spread matrix.

The first minimum of the GAF occurs approximately when

$$Q(\Delta A) \triangleq \Delta A^T M \Delta A \cong 1. \tag{26}$$

Equation (26) measures the extent of the GAF's main lobe.

After algebraic computations

$$M_{ij} = M_{0_{ij}} - M_{1_{ij}} \tag{27}$$

with

$$M_0 = [M_{0_{ij}}] = \left(\frac{2\pi}{\lambda}\right)^2 \frac{1}{2X}\int_{-X}^{X} [\nabla_{A_a} R(l, A)] \cdot [\nabla_{A_a} R(l, A)]^T \, dl \tag{28}$$

and

$$M_1 = [M_{1_{ij}}] = \left(\frac{2\pi}{\lambda}\right)^2 \left[\frac{1}{2X}\int_{-X}^{X} \nabla_{A_a} R(l, A)\, dl\right] \cdot \left[\frac{1}{2X}\int_{-X}^{X} \nabla_{A_a} R(l, A)\, dl\right]^T. \tag{29}$$

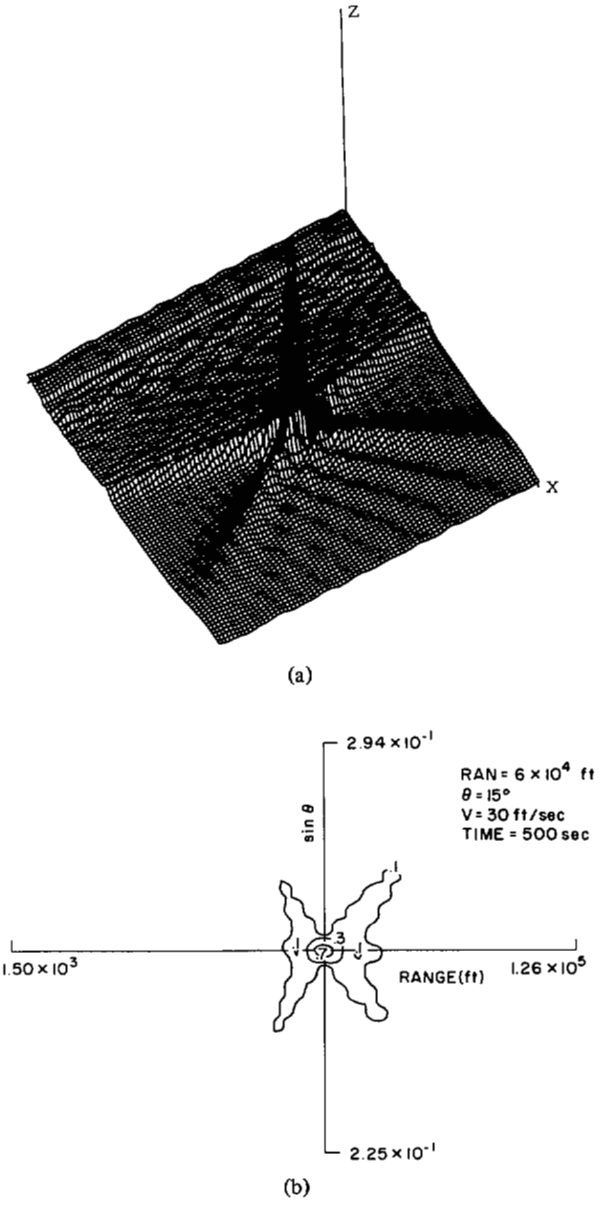

Fig. 6. SOSS ambiguity structure: (a) Three-dimensional plot. (b) Contour plot.

In (28) and (29) ∇_{A_a} is the gradient column vector operator with respect to the parameter vector A, evaluated at the source location $A = A_a$. Apart from scaling factors, the elements of M depend exclusively on the bearing angle and on the geometric parameter $X = L/2R_0$.

Although (28) and (29) may be integrated [12], due to their analytical complexity, the closed form expressions obtained are of little practical relevance. Rather, local, asymptotic, and graphical studies with respect to X are pursued. However, since in section V the interest lies on the inverse M^{-1}, the det M, and the cross correlation $\rho_{R \cdot \sin\theta}$, the subsequent analysis concentrates on these entities.

A. Distant Observer (Local Analysis) (Fresnel Zone)

For a distant observer geometry, i.e., when $X = L/2R_0 < 1$, a Taylor series study in X is pursued. Truncation after the

first nonzero order term leads to

$$M^{-1} \cong \left(\frac{\lambda}{2\pi}\right)^2 \left[\begin{array}{c:c} 45/\cos^4 \theta X^4 & -33 \sin \theta/R_0 \cos^2 \theta X^2 \\ \hdashline = & 3/R_0{}^2 X^2 \end{array}\right] \tag{30}$$

$$\det M \cong (2\pi/\lambda)^4 R_0{}^2 \cos^4 \theta X^6/3^3 \times 5 \tag{31}$$

$$\rho_{R_0 \sin \theta} = (M^{-1})_{12}/[(M^{-1})_{11}(M^{-1})_{22}]^{1/2} \tag{32}$$

$$\cong -11 \sin \theta X/\sqrt{15}. \tag{33}$$

B. Close Observer (Asymptotic Analysis)

Neglecting the amplitude attenuation effects across the observing array, the asymptotic analysis is restricted to the phase information. As $X \to \infty$

$$M^{-1} \cong \left(\frac{\lambda}{2\pi}\right)^2 \left[\begin{array}{c:c} \frac{2}{\pi}\cos \theta X - \cos 2\theta & \sin 2\theta \left(\frac{X}{\pi} - \cos \theta\right)\Big/ R_0 \\ \hdashline = & \left(\frac{2}{\pi}\cos \theta \sin^2 \theta X + \cos^2 \theta \cos 2\theta\right)\Big/ R_0{}^2 \end{array}\right] \tag{34}$$

$$\det M \cong \left(\frac{2\pi}{\lambda}\right)^4 R_0{}^2 \pi \Big/ 2 \cos \theta X \tag{35}$$

and

$$\rho_{R_0 \sin \theta}{}^2 \cong 1 - \pi/2 \sin^2 \theta \cos \theta X, \qquad \theta \neq 0, \frac{\pi}{2}. \tag{36}$$

For large synthetic arrays the receiver is highly sensitive to the relative geometry. The cross correlation for $\theta \neq 0, \pi/2$ tends asymptotically to 1 and M becomes singular. Intuitively this behavior reflects that, from phase information and for an infinitely large array, the identifiable parameter is the distance $R_0 \cos \theta$ from the source to the observer.

C. Graphical Representations

The exact closed form expressions for the diagonal elements of M^{-1} are presented in Figs. 7 and 8 as functions of X.

The nominal conditions assumed are $R_0 = 6 \times 10^4$ ft, $\theta = 15°$. The figures also display the local and asymptotic tangent equations (30) and (34), respectively.

Observe the quadratic (convex cup) behavior of the range and bearing mean-square spreads. It reflects two different phenomena: the main-lobe flatness and shearing. For small X (distant observer) the main lobe is spread out at the origin (source location) corresponding to large uncorrelated inverses of the second-order derivatives of the GAF. As X increases the main lobe gets sharper, but a shearing effect occurs leading to a cross correlation which decreases monotonically to -1. As a consequence, the spread functions (diagonal elements of M^{-1}) attain a minimum at a certain value of X (dependent on the relative geometry) and then increase monotonically.

VI. MEAN-SQUARE PERFORMANCE

Section IV described a two-stage implementation of the ML receiver, consisting of a crude search followed by a finer one. Global acquisition of the source parameters is performed by the first step of the algorithm. This section studies the errors associated with the range and the bearing estimates, concentrating on a mean-square performance analysis.

A. Cramer-Rao Bounds

For the model described in section III, a lower bound to the mean-square error is given by the Cramer-Rao inequality

$$\Lambda_\epsilon = E[(A_{ml} - A_a)(A_{ml} - A_a)^*] \geqslant J^{-1} \tag{37}$$

where J is the Fisher information matrix

$$J = -E\left[\frac{\partial^2 \ln \Lambda_1(A)}{\partial A_i \partial A_j}\bigg|_{A=A_a}\right]. \tag{38}$$

Under general regularity conditions, satisfied by this parameter estimation problem

$$J = GM \tag{39}$$

with M defined by (25) and

$$G = 2\frac{\bar{E}_r}{N_0}\frac{\bar{E}_r}{N_0 + \bar{E}_r}. \tag{40}$$

B. Total Bounds

Let A_j represent the jth component of the source parameter vector A. The mean-square error on the estimate $A_{j_{ml}}$ is

$$\sigma_{tot_j}{}^2 = E(A_{j_\epsilon}{}^2) = E(A_j - A_{j_{ml}})^2 = \sigma_{gl_j}{}^2 + \sigma_{loc_j}{}^2 \tag{41}$$

where the global and local mean-square error components are

$$\sigma_{gl_j}{}^2 = E(A_j{}^2 \mid \xi) \Pr(\xi) \tag{42}$$

$$\sigma_{loc_j}{}^2 = E(A_{j_\epsilon}{}^2 \mid \xi^c)[1 - \Pr(\xi)]. \tag{43}$$

In (42) and (43) ξ is the event that a decision error or diversion occurs, i.e., that the first step of the algorithm returns the wrong grid vertex; ξ^c is the complement of ξ; and $\Pr(\xi)$ is the probability of the event ξ.

The computation of the various quantities in (41) to (43) depends on the design and dimension of the grid discretizing the parameter space. Assuming that the grid cells are the ellipses determined by (26), from the negligible side-lobe structure of the ambiguity function, it follows that the coarse

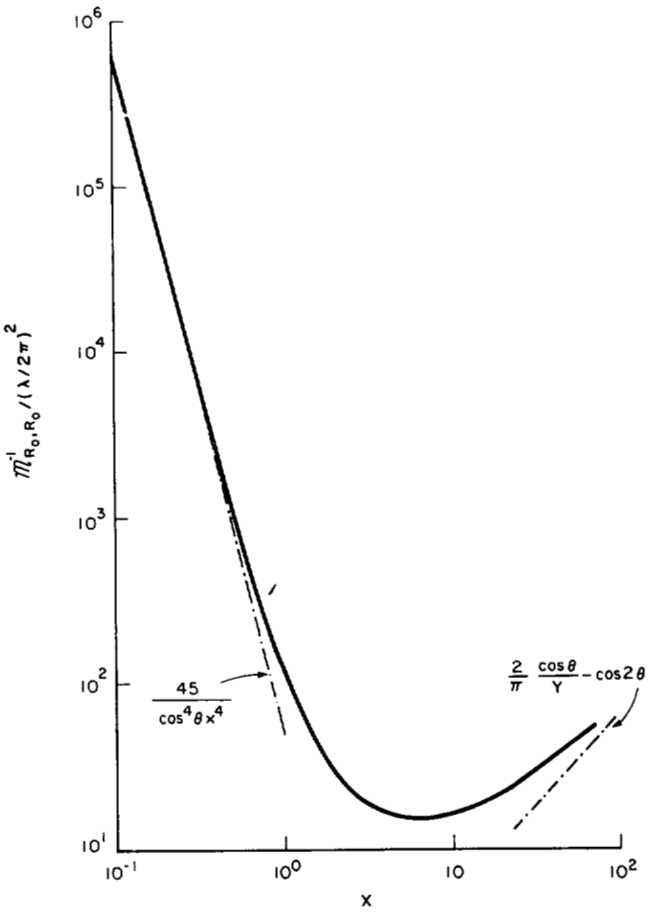

Fig. 7. Inverse range mean-square spread versus $X = L/2\,R_0$.

search step is equivalent to a multiple-hypothesis decision-testing problem with M orthogonal signals transmitted over a Rayleigh channel.

The *a priori* unknown source location is restricted to a rectangular region Ω, and

$$\Omega = \overset{2}{\underset{j=1}{X}} [A_{j_m}, A_{j_M}] = [R_{0_m}, R_{0_M}]\, X\, [\sin\theta_m, \sin\theta_M]\,. \tag{44}$$

For large-energy signal-to-noise ratio and large number M of grid cells, the probability of error is

$$\Pr(\xi) \cong \left(\ln M - \frac{1}{2M} + \gamma\right) \Big/ (E_r/N_0) \tag{45}$$

and the conditional mean-square error

$$E(A_j{}^2 \mid \xi) = \frac{(\Delta_M A_j)^2}{6} \tag{46}$$

where $\Delta_M A_j = A_{j_M} - A_{j_m}$ and γ is the Euler constant. In (45) M is given by

$$M = \frac{V_\Omega}{\pi} (\det \mathsf{M})^{1/2} \tag{47}$$

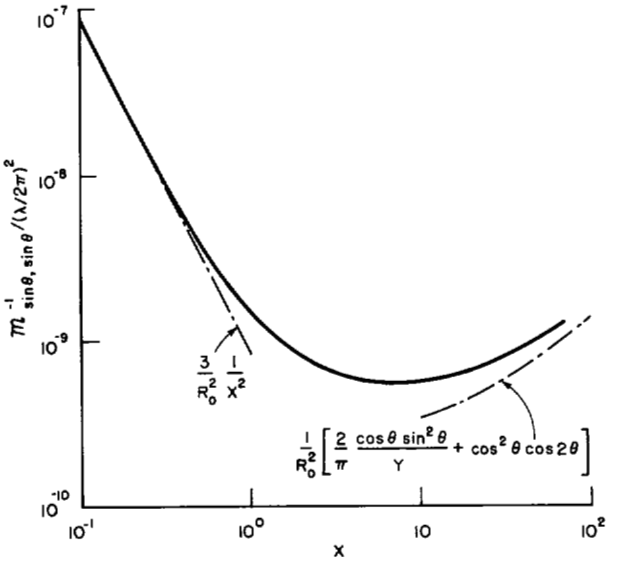

Fig. 8. Inverse bearing mean-square spread versus $X = L/2\,R_0$.

where V_Ω is the volume of Ω, computed from (44).

Finally $E(A_j{}^2 \mid \xi^c)$ is approximated by the Cramer-Rao inequality (37).

Substituting (30) and (31), or (34) and (35) in (42)-(47), and these in (41) lead to analytical expressions for the mean-square errors for the distant and close observer geometries, respectively.

C. Graphical Analysis

Figs. 9 and 10 illustrate the range and bearing total mean-square performance as functions of the geometric parameter X. The geometrical and statistical conditions assumed are as follows:

$$R_0 = 6 \times 10^4 \text{ ft}$$

$$\theta = 15^\circ$$

SNR = signal-to-noise ratio = 0 dB

$$\Delta_M R_0 = 6 \times 10^5 \text{ ft}$$

$$\Delta_M = 5^\circ$$

$$\sigma_b{}^2 = \frac{1}{2}$$

$$\lambda = 50 \text{ ft}.$$

The *a priori* range uncertainty $\Delta_M R_0$ is ten times the actual range R_0; however, it follows from Fig. 9 that the ML algorithm can focus globally the range parameter, i.e., it achieves $\sigma_{R_0} \ll R_0$.

For $X_1 \cong 10^{-2}$, the standard deviation for the range-estimation error is about 7.5 percent of R_0, while for $X_2 \cong 10^{-1}$ (a ten times larger array), it is reduced to only 5 percent of R_0. This results from the fact that for smaller X, the local errors dominate the global ones, while for larger X, it is the contrary; as X increases the total errors depart from the

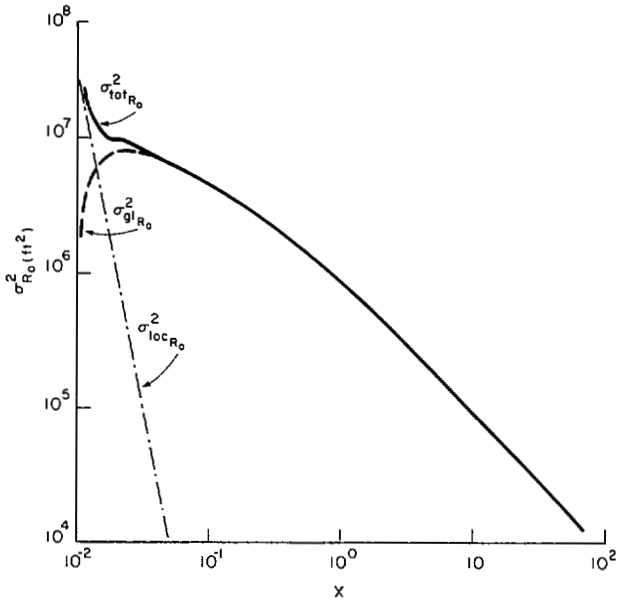

Fig. 9. Total range mean-square error versus $X = L/2\,R_0$.

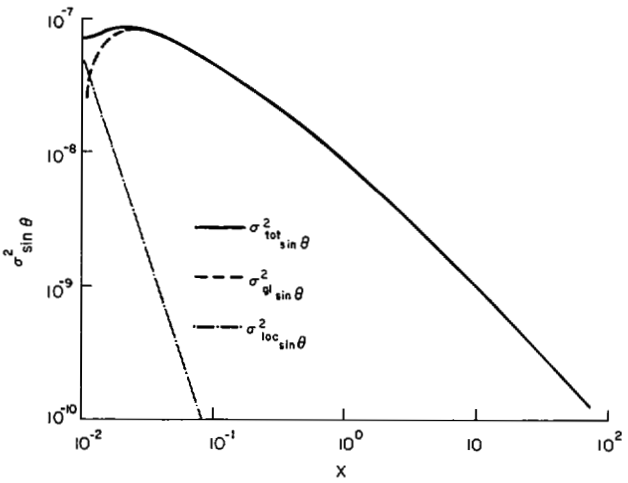

Fig. 10. Total bearing mean-square error versus $X = L/2\,R_0$.

Cramer-Rao bounds and approach the global mean-square error components, with a logarithm-type decaying.

Being independent of the statistical background, the behavior observed is the sole reflexion of the geometry on the performance. In fact the following is true:

1) The increase in X sharpens the main lobe; maintaining the *a priori* uncertainty, it enlarges the total number of grid cells augmenting Pr (ξ).

2) A change in SNR affects only the scaling of the ordinate axis, or, equivalently, just implies a parallel translation of the curves. This pattern of variation is characteristic of the Rayleigh model assumed and of the two-step algorithm. In practice, as it happens with active radar, the problem is circumvented by resorting to multiple independent observations (e.g., finite coherence time); the estimation procedure described is then efficient in the SNR sense.

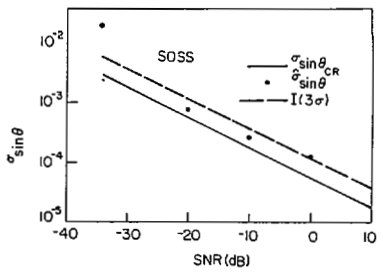

Fig. 11. Range Monte Carlo simulation results.

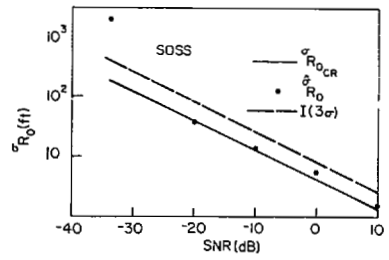

Fig. 12. Bearing Monte Carlo simulation results.

The stationary observer/stationary source passive-tracking problem was simulated in a digital computer, for a configuration where

$$R_0 = 6 \times 10^3$$

$$\theta = 0^\circ$$

$$\lambda = 50 \text{ ft}$$

$$\sigma_b^2 = 1$$

$$X = .331$$

$$T = 1 \text{ s}$$

and the inter-spacing between the array elements was $\Delta L = \lambda/2$.

For several SNR values, Figs. 11 and 12 study the convergence between the theoretical performance and the results of Monte Carlo simulations. They exhibit a threshold phenomenon, since for SNR > -30 dB the statistical results are within the three-variance confidence interval $I\,(3\sigma)$ of the Cramer-Rao bounds, while the point SNR $= -34$ dB is about one order of magnitude apart from the Cramer-Rao bound.

VII. CONCLUSION

A model has been presented encompassing the global and local characteristics of the passive-tracking problem. It exhibits global observability for both the range and the bearing. The parameters are demodulated from the wavefront curvature, e.g., as sensed by a spatially extended observer. Underlying all the work presented is the absence of the far-field (planar wavefront) assumption.

The ambiguity structure and the theoretical and practical limitations on the mean-square performance have been analyzed. For a distant observer geometry (Fresnel zone) the estimation errors are practically uncoupled; the statistical mean-square performance follows closely the values predicted by the Cramer-Rao bounds. The bearing estimation depends on the linear effects (e.g., linear delay across the array or observed Doppler), while the range focusing is achieved from the second-order modulations (spherical curvature or chirp modulation). As the geometry changes from broadside ($\theta = 0^\circ$) to endfire ($\theta = \pi/2$), the range performance deteriorates due to the reduction of the effective array length. For larger values of X, the two-step implementation of the ML receiver exhibits threshold effects, with the global errors dominating the mean-square error performance.

The work was not restricted to high SNR's, and remains valid even for large *a priori* uncertainty. However, the Monte Carlo simulations suggested a lower bound on the SNR, around -30 dB, below which the analysis is significantly misleading, i.e., the bounds are not tight.

The model assumed a highly coherent signal disturbed by incoherent noise components. Nevertheless, the results reflecting the geometry on the mean-square performance and the receiver structure are still valid for more general signal models [12]. This is true whenever the statistical and the geometrical effects factor as in (11).

In Part II [14] an omnidirectional observer acquires a source moving along a deterministic path. The range, speed, and bearing defining the source/receiver geometry are measured by exploring the temporal diversity induced on the received signals. In Part III [15] configurations are considered, where a spatially extended observer tracks a moving source. The paper concentrates on the study of the resulting space/time coupled processing.

REFERENCES

[1] R. W. Bass, R. E. Mortensen, V. D. Norum, B. Shawaf, and H. W. Sorenson, "ASW target motion and measurement models," CSA Tech. Rep., 72-024-01, Sept. 1972.

[2] Beckmann and Spizzichino, *Scattering of Electromagnetic Waves from Rough Surfaces.* New York, Pergamon, 1963.

[3] A. B. Baggeroer, "High resolution velocity/depth spectra estimation for seismic profiling," in *IEEE Int. Conf. Eng Ocean Environ.*, vol. II, 1974.

[4] W. J. Bangs, "Array processing with generalized beam-formers," doctoral thesis, Yale Univ., New Haven, CN, Sept. 1971.

[5] W. J. Bangs and P. M. Schultheiss, "Space-time processing for Optimal Parameter Estimation," in *Signal Processing*, J. W. R. Griffiths, P. L. Stocklin, and C. Van Schooneveld, Eds. New York: Academic Press, 1973.

[6] L. S. Cahoon and M. J. Hinich, "A method for locating targets using range only," *IEEE Trans. Inform. Theory*, vol. IT-22, pp. 217–225, Mar. 1976.

[7] M. A. Gallop and L. W. Nolte, 'Bayesian detection of targets of unknown location," *IEEE Trans. Aerosp. Electron. Syst.*, vol. AES-10, pp. 429-435, 1974.

[8] *Proc. IEEE, Special Issue on Rays and Beams*, vol. 62, pp. 1409–1618, Nov. 1974.

[9] *IEEE Trans. Geosci. Electron., Special Issue on Data Collection from Multiple Earth Platforms*, vol. GE-13, Jan. 1975.

[10] K. D. McDonald, "A survey of satellite-based systems of navigation, position surveillance, traffic control and collission avoidance," *Navigation: J. Inst. Navigation*, vol. 20, no. 4, Winter, 1973–74.

[11] T. P. McGarty, "The effect of interfering signals on the performance of angle of arrival estimates," *IEEE Trans. Aerosp. Electron. Syst.*, vol. AES-10, pp. 70–77, 1974.

[12] J. M. F. Moura, "Passive systems theory with applications to positioning and navigation," doctoral thesis, M. I.T., June 1975. —, R.L.E. Rep. no. 490, M.I.T., Cambridge, MA, Apr. 28, 1976.

[13] J. M. F. Moura, H. L. Van Trees, and A. B. Baggeroer, "Space time tracking by a passive observer," 4th Symp. on Nonlinear Estimation Theory and Its Applications, San Diego, CA., Sept. 1973.

[14] J. M. F. Moura, "Passive systems theory with narrow-band and linear constraints. Part II: Temporal diversity," to be submitted for publication.

[15] J. M. F. Moura, "Passive systems theory with narrow-band and linear constraints. Part III: Spatial/temporal diversity," to be submitted for publication.

[16] A. Papoulis, *Systems and Transforms with Applications in Optics.* New York: McGraw-Hill, 1967.

[17] L. P. Seidman, "Bearing estimation with a linear array," *IEEE Trans. Audio and Electroacoust.*, vol. AU-19, pp. 147–157, 1971.

[18] R. C. Spindel and R. P. Porter, "Precision tracking systems for sonobuoys," in *IEEE Int. Conf. Eng. Ocean Environ.*, vol. II, 1974.

[19] M. T. Taner and F. Koehler, "Velocity spectra-digital computer derivation and applications of velocity function," *Geophys*, vol. 34, no. 6, pp. 859–881, Dec. 1969.

[20] H. L. Van Trees, *Detection, Estimation and Modulation Theory: Part II.* New York: Wiley, 1971.

[21] E. E. Westerfield, "Determination of position of a drifting buoy by means of the Navy navigation satellite system," in *IEEE Conf. Eng. Ocean Environ.*, pp. 443–446, 1972.